

## LARGE-SCALE DYNAMOS AT LOW MAGNETIC PRANDTL NUMBERS

AXEL BRANDENBURG

NORDITA, AlbaNova University Center, Roslagstullsbacken 23, SE-10691 Stockholm, Sweden  
*Draft version November 12, 2018*

### ABSTRACT

Using direct simulations of hydromagnetic turbulence driven by random polarized waves it is shown that dynamo action is possible over a wide range of magnetic Prandtl numbers from  $10^{-3}$  to 1. Triply periodic boundary conditions are being used. In the final saturated state the resulting magnetic field has a large-scale component of Beltrami type. For the kinematic phase, growth rates have been determined for magnetic Prandtl numbers between 0.01 and 1, but only the case with the smallest magnetic Prandtl number shows large-scale magnetic fields. It is less organized than in the nonlinear stage. For small magnetic Prandtl numbers the growth rates are comparable to those calculated from an alpha squared mean-field dynamo. In the linear regime the magnetic helicity spectrum has a short inertial range compatible with a  $-5/3$  power law, while in the nonlinear regime it is the current helicity whose spectrum may be compatible with such a law. In the saturated case, the spectral magnetic energy in the inertial range is in slight excess over the spectral kinetic energy, although for small magnetic Prandtl numbers the magnetic energy spectrum reaches its resistive cut off wavenumber more quickly. The viscous energy dissipation declines with the square root of the magnetic Prandtl number, which implies that most of the energy is dissipated via Joule heat.

*Subject headings:* MHD – turbulence

### 1. INTRODUCTION

Many astrophysical plasmas are turbulent and tend to be magnetized. The magnetic fields can have typical length scales that are either larger or smaller than that of the energy-carrying eddies. We speak then correspondingly of large-scale or small-scale dynamos. Small-scale dynamos can already work in statistically mirror-symmetric isotropic homogeneous turbulence, whereas large-scale dynamos require in general a departure from parity-invariant or mirror-symmetric flows. The excitation conditions of small-scale dynamos depend sensitively on the value of the magnetic Prandtl number, i.e. the ratio of kinematic viscosity to magnetic diffusivity,  $Pr_M = \nu/\eta$ , where  $\nu$  is the kinematic viscosity and  $\eta$  the magnetic diffusivity. This sensitivity is related to the fact that in the *kinematic* regime the spectral magnetic energy is peaked at the resistive scale. As was pointed out originally by Rogachevskii & Kleeorin (1997), and more recently by Boldyrev & Cattaneo (2004), the slope of the kinetic energy spectrum is important for the onset of small-scale dynamo action. It matters therefore whether the resistive scale lies in the viscous range ( $Pr_M \approx 1$ ), within the inertial range ( $Pr_M \lesssim 0.1$ ), or right within the range where the bottleneck occurs ( $Pr_M \approx 0.1$ ). The bottleneck effect refers to the spectral subrange just before the dissipation range where the kinetic energy spectrum is shallower than in the inertial range. Within the bottleneck range the velocity increments diverge even more strongly with decreasing separation than in the inertial range, making dynamo action harder still. Indeed, for small values of  $Pr_M$  the critical value of the magnetic Reynolds number above which small-scale dynamo action occurs increases therefore sharply toward  $Pr_M = 0.1$  (Schekochihin et al. 2005), and then decreases slightly for  $Pr_M < 0.05$  (Iskakov et al. 2007). However, even with the computing power available today, direct simulations of small-scale dynamo action are still only marginally possible at such small values of  $Pr_M$ .

For certain types of flows dynamo action is easier to achieve

even though  $Pr_M$  is small. The Taylor-Green flow is an example where the critical value of the magnetic Reynolds number becomes constant for  $Pr_M < 0.1$  (Ponty et al. 2004, 2005). In this flow there can be large-scale patches with finite kinetic helicity of opposite sign. A completely different example is fully helical turbulence where the excitation condition for dynamo action is virtually unchanged as  $Pr_M$  decreases from 1 to 0.1 (Brandenburg 2001, hereafter B01). For an ABC-flow dynamo, Mininni (2007) found a weak dependence of the threshold value of the magnetic Reynolds number  $Re_M$  on  $Pr_M$ . For  $Pr_M < 0.1$  the threshold value seemed to become asymptotically independent of  $Pr_M$  and dynamo action was demonstrated for values of  $Pr_M$  down to  $5 \times 10^{-3}$ .

In many astrophysical bodies,  $Pr_M$  is indeed rather small (around  $10^{-5}$ ). Such systems still possess dynamo action and can have large-scale magnetic fields. It is likely that such systems belong to the second class of systems where the excitation conditions are not drastically altered toward small values of  $Pr_M$ . Indeed, large-scale magnetic fields are found regardless of whether  $Pr_M$  is small (e.g., the Sun and other stars with outer convection zones, as well as planets) or large (e.g., in spiral galaxies, because of their low densities).

The purpose of this paper is to point out that a strong  $Pr_M$  dependence does not occur in systems where the magnetic field generation is predominantly due to a large-scale dynamo. Such systems have been studied in idealized settings such as periodic boxes using explicit forcing functions for driving the turbulence. This has significant advantages in that periodic boundary conditions can be used, energy spectra are easily computed and, most importantly, isotropy and homogeneity eases comparison with turbulence theory. A disadvantage is that the magnetic helicity can only change on resistive timescales, which slows down the saturation (B01).

With these provisions in mind, we consider now simulations of maximally helical turbulence in triply periodic boxes where we keep in most cases the fluid Reynolds number,  $Re = u_{rms}/\nu k_f$ , constant and vary the magnetic Reynolds number,  $Re_M = u_{rms}/\eta k_f$ , and thereby  $Pr_M (\equiv Re_M/Re)$ . Here,

$u_{\text{rms}}$  is the rms velocity of the turbulence and  $k_f$  is the forcing wavenumber. According to B01 the dynamo should be excited whenever the domain is large enough (2–3 times larger than the forcing scale) and the magnetic Reynolds number exceeds unity ( $\text{Re}_M \geq 1.1\dots 1.4$  or so). This was confirmed for magnetic Prandtl numbers as low as 0.1. In the present work we consider kinematic dynamo action down to values of  $\text{Pr}_M = 10^{-2}$  and nonlinear saturated dynamos down to  $\text{Pr}_M = 10^{-3}$ .

## 2. THE METHOD

We solve the hydromagnetic equations for velocity  $\mathbf{U}$ , logarithmic density  $\ln \rho$ , and magnetic vector potential  $\mathbf{A}$  for an isothermal gas in the presence of an externally imposed helical forcing function  $\mathbf{f}$ ,

$$\frac{\partial \mathbf{U}}{\partial t} = -\mathbf{U} \cdot \nabla \mathbf{U} - c_s^2 \nabla \ln \rho + \mathbf{f} + \rho^{-1} (\mathbf{J} \times \mathbf{B} + \nabla \cdot 2\rho \nu \mathbf{S}), \quad (1)$$

$$\frac{\partial \ln \rho}{\partial t} = -\mathbf{U} \cdot \nabla \ln \rho - \nabla \cdot \mathbf{U}, \quad (2)$$

$$\frac{\partial \mathbf{A}}{\partial t} = \mathbf{U} \times \mathbf{B} - \mu_0 \eta \mathbf{J}. \quad (3)$$

Here,  $\mathbf{B} = \nabla \times \mathbf{A}$  is the magnetic field,  $\mathbf{J} = \nabla \times \mathbf{B} / \mu_0$  is the current density,  $\mu_0$  is the vacuum permeability,  $c_s$  is the isothermal speed of sound, and  $\mathbf{S}_{ij} = \frac{1}{2}(U_{i,j} + U_{j,i}) - \frac{1}{3}\delta_{ij}\nabla \cdot \mathbf{U}$  is the traceless rate of strain tensor. We consider a triply periodic domain of size  $L^3$ , so the smallest wavenumber in the domain is  $k_1 = 2\pi/L$ . The forcing function consists of eigenfunctions of the curl operator with positive eigenvalues and is therefore fully helical with  $\mathbf{f} \cdot \nabla \times \mathbf{f} = k_f^2$ , where  $3.5 \leq k/k_1 \leq 4.5$  is wavenumber interval of the forcing function, whose average value is referred to as  $k_f = 4k_1$ . The amplitude of  $\mathbf{f}$  is such that the Mach number is  $u_{\text{rms}}/c_s \approx 0.1$ , so compressive effects are negligible (Dobler et al. 2003).

The initial conditions consist of a weak Beltrami field. The initial velocity is zero and the initial density is uniform with  $\rho = \rho_0 = \text{const}$ . Note that the volume-averaged density remains constant, i.e.,  $\langle \rho \rangle = \rho_0$ .

The model is equivalent to that of B01, except that there the value of  $k_f/k_1$  was chosen to be either 5 or 30. In order for large-scale dynamo action to be possible,  $k_f/k_1$  must at least be larger than 2 (Haugen et al. 2004), but 3 is already sufficient (Brandenburg et al. 2008). In the kinematic regime the fastest growing mode is expected to have the wavenumber  $k_f/2$ , so in order that this wavenumber is distinct from  $k_1$ , we have chosen  $k_f/k_1 = 4$  throughout this paper.

## 3. RESULTS

We begin by presenting results for  $\text{Re} \approx 670$  where we vary  $\text{Pr}_M$  in the range  $0.01 \leq \text{Pr}_M \leq 1$ , i.e.,  $\text{Re}_M$  is varied in the range  $6.7 \leq \text{Re}_M \leq 670$ . The dynamo is excited in all those cases, but the growth rate  $\lambda$  varies. We consider first the kinematic regime where the magnetic field is weak and turn then to the nonlinear regime where the magnetic field has saturated. Most of the results presented below have been obtained at a resolution of  $512^3$  meshpoints. The solution was first evolved at lower resolution ( $128^3$  meshpoints), then remeshed to twice the resolution, again evolved for some time, and finally remeshed to  $512^3$  meshpoints, and again evolved for some time. Data for the kinematic regime are only used after the initial transients have disappeared and a clear exponential growth has developed at all length scales for at least some

40 turnover times (also for the runs with a resolution of  $512^3$  meshpoints). The run with  $128^3$  meshpoints has been evolved all the way into saturation, and it was then remeshed twice by a factor of 2, just like in the kinematic regime.

### 3.1. Field structure in the kinematic regime

Visualizations of one component of the magnetic field show the emergence of a large-scale magnetic field for small values of  $\text{Pr}_M$ . This is clearly demonstrated in Fig. 1, where we see for  $\text{Pr}_M = 0.01$  a large-scale pattern with a systematic variation in the  $y$  direction. For  $\text{Pr}_M = 0.1$  there is no such variation, although there are some extended patches in which the field orientation is the same. For  $\text{Pr}_M = 1$  even this is no longer the case and the field appears completely random with small-scale variations only.

We emphasize that random and patch-like structures only occur in the kinematic regime. In the saturated regime a large-scale field emerges in all cases. This will be discussed in §3.7.

### 3.2. Growth rates

The growth rate is calculated as the average of the instantaneous growth rate,  $d \ln B_{\text{rms}}/dt$ . Examples are shown in Fig. 2 for runs with  $\text{Re} = 670$  and different values of  $\text{Pr}_M$  using  $512^3$  meshpoints. In Fig. 3, we show growth rates normalized by  $u_{\text{rms}}k_f$  (inverse turnover times) as a function of  $\text{Re}_M$  for three values of  $\text{Re}_M$  and compare with the corresponding results for non-helical turbulence forced at larger scales in the wavenumber interval  $1 \leq k/k_1 \leq 2$  (Haugen et al. 2004). In that case we use  $k_f = 1.5$  for the average value. The small-scale dynamo is then only excited when  $\text{Re}_M \geq 35$ . For  $\text{Re}_M \geq 100$  the growth rates for helical turbulence with  $k_f = 4$  are quite similar to those of non-helical turbulence with  $k_f = 1.5$ . We have also calculated growth rates for the non-helical case with  $k_f = 4$  and find the same values as in the helical case. We note that in all cases, and even for small values of  $\text{Pr}_M$ , the growth rates based on the rms magnetic field are equal to those based on the rms values of the mean fields obtained by averaging over any two coordinate directions.

In both helical and non-helical cases, when  $\text{Re}_M$  is large enough,  $\lambda$  increases like  $\text{Re}_M^{1/2}$ , as expected (Schekochihin et al. 2004). This is because the eddy turnover rate at the resistive scale is  $\propto k_\eta^{2/3}$ , but because  $k_\eta/k_f \propto \text{Re}_M^{3/4}$  we have  $\lambda \propto \text{Re}_M^{1/2}$ . However, when there is also large-scale dynamo action, one expects there to be a lower bound for  $\lambda$  given by the growth rate for the large-scale dynamo,  $\lambda_{\text{LS}}$ . Using the theory for an  $\alpha^2$  dynamo (Moffatt 1978, Krause & Rädler 1980), we have

$$\lambda_{\text{LS}} = |\alpha k| - (\eta + \eta_t)k^2, \quad (4)$$

where  $\alpha$  is a pseudo scalar (the  $\alpha$  effect) and  $\eta_t$  is the turbulent magnetic diffusivity. For fully helical turbulence we have  $|\alpha| \approx u_{\text{rms}}/3$  and  $\eta_t \approx u_{\text{rms}}/3k_f$  (Sur et al. 2008), so we can write the growth rate as

$$\frac{\lambda_{\text{LS}}}{u_{\text{rms}}k_f} = \frac{1}{3} \frac{k_1}{k_f} \left[ 1 - \frac{k_1}{k_f} (1 + 3\text{Re}_M^{-1}) \right], \quad (5)$$

where we have put  $|k| = k_1$ . Over the parameter range considered in this paper ( $\text{Re}_M \geq 6.7$  and  $k_f/k_1 = 4$ ),  $\lambda_{\text{LS}}/u_{\text{rms}}k_f$  increases only slightly from 0.053 to 0.062 as  $\text{Re}_M$  increases.

The result shown in Fig. 3 gives values that are systematically below  $\lambda_{\text{LS}}$ . There could be two reasons for this discrepancy. On the one hand, the accuracy of the estimates

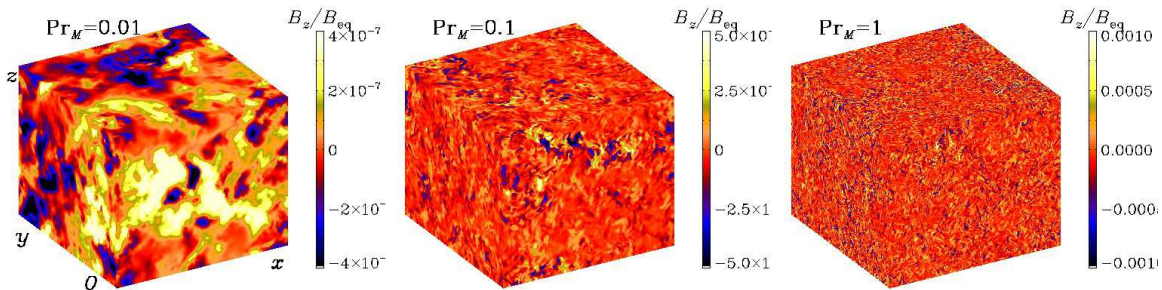


FIG. 1.— Visualization of  $B_z$  for  $\text{Pr}_M = 0.01, 0.1,$  and  $1$  at  $\text{Re} = 670$ . Note the emergence of a large-scale pattern for  $\text{Pr}_M = 0.01$ . For  $\text{Pr}_M = 0.1$  there are only a few extended patches and for  $\text{Pr}_M = 1$  the field is completely random and of small scale only. The orientation of the axes is indicated for the first panel, and is the same for all other panels.

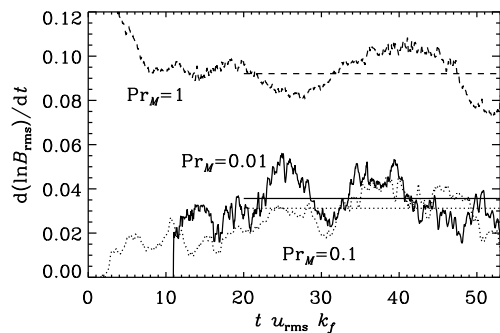


FIG. 2.— Instantaneous growth rate for runs with different values of  $\text{Pr}_M$  and  $512^3$  meshpoints. The straight lines give the growth rates obtained by averaging over the indicated time interval. The solid, dotted, and dashed lines are for  $\text{Pr}_M = 0.01, 0.1,$  and  $1$ , respectively.

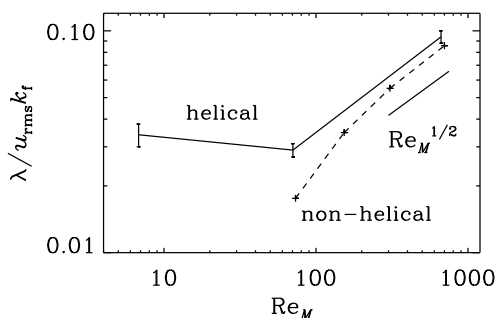


FIG. 3.— Dynamo growth rates of the rms magnetic field for helical turbulence with  $\text{Re} = 670$  (solid line) compared with growth rates for non-helical turbulence (dashed lines; adapted from Haugen et al. 2004).

$|\alpha| \approx u_{\text{rms}}/3$  and  $\eta_i \approx u_{\text{rms}}/3k_f$  may not be good enough. On the other hand, equation (4) is only an approximation in cases where  $\lambda_{\text{LS}} \neq 0$ , because then memory effects become important. This means that, when allowing  $\alpha$  and  $\eta_i$  to be integral kernels in time, they are no longer proportional to  $\delta$  functions, but have finite widths in time. This effect has recently been studied by Hubbard & Brandenburg (2008) and can be quite dramatic in some cases.

In Fig. 3, we have varied  $\text{Re}_M$  by changing  $\text{Pr}_M$  and keeping  $\text{Re} = \text{const} = 670$ . We can therefore also consider this graph as a representation of the magnetic Prandtl number de-

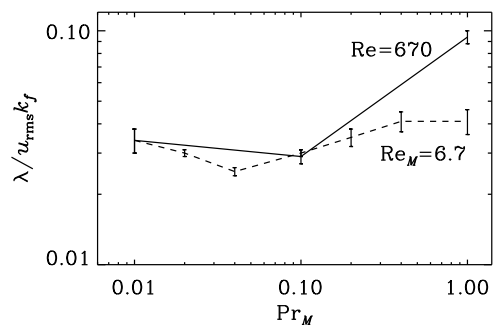


FIG. 4.— Dependence of dynamo growth rates of the rms magnetic field on  $\text{Pr}_M$  for helical turbulence with  $\text{Re}_M = 6.7$  (dashed line) and  $\text{Re} = 670$  (solid line). Here the solid line corresponds to the solid line in Fig. 3.

pendence of  $\lambda$ . However,  $\text{Pr}_M$  can also be changed while keeping  $\text{Re}_M = \text{const} = 6.7$ . The corresponding result is shown in Fig. 4 and compared with the previous case. The two graphs are in reasonable agreement for small values of  $\text{Pr}_M$ , but the rise of  $\lambda$  for  $\text{Re} = 670$  around  $\text{Pr}_M = 1$  is not seen in the case with  $\text{Re}_M = 6.7$ . This suggests that the transition from a purely large-scale turbulent dynamo to a mixed large-scale and small-scale turbulent dynamo requires values of  $\text{Re}_M$  above some critical value (somewhere between 10 and 100), and is not just determined by the value of  $\text{Pr}_M$ .

### 3.3. Spectra

The transition from a purely large-scale turbulent dynamo to a mixed large-scale and small-scale turbulent dynamo is accompanied by characteristic changes in the spectral properties of the magnetic field. In the following we employ shell-integrated spectra of kinetic and magnetic energy,  $E(k)$  and  $M(k)$ , respectively, as well as of kinetic and magnetic helicities,  $F(k)$  and  $H(k)$ , respectively. These spectra are normalized such that  $\int E(k) dk = \frac{1}{2} \langle U^2 \rangle \equiv E$ ,  $\int M(k) dk = \frac{1}{2} \langle B^2 \rangle \equiv M$ ,  $\int F(k) dk = \langle \mathbf{W} \cdot \mathbf{U} \rangle$ , and  $\int H(k) dk = \langle \mathbf{A} \cdot \mathbf{B} \rangle$ , where  $\mathbf{W} = \nabla \times \mathbf{U}$  is the vorticity.

In Fig. 5, we plot  $E(k)$  and  $M(k)$  for three cases with  $\text{Pr}_M = 1, 0.1,$  and  $0.01$ , keeping  $\text{Re} = 670$  in all cases. The magnetic energy spectra are compensated by  $\exp(-\lambda t)$ , where  $\lambda$  is the numerically determined growth rate for each run, and then averaged in time. We consider here only the kinematic regime when the magnetic energy is weak. The kinetic energy spectra are then always the same. Since the magnetic energy is weak, we have scaled the magnetic energy spectra for differ-

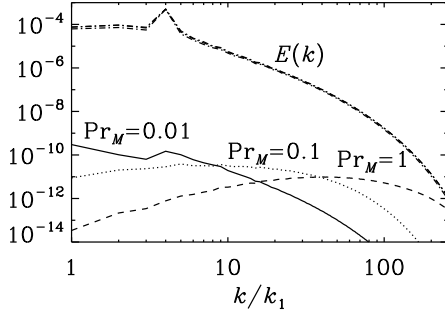


FIG. 5.— Spectra of kinetic and magnetic energies in the kinematic regime for  $\text{Pr}_M = 0.01, 0.1,$  and  $1$ .

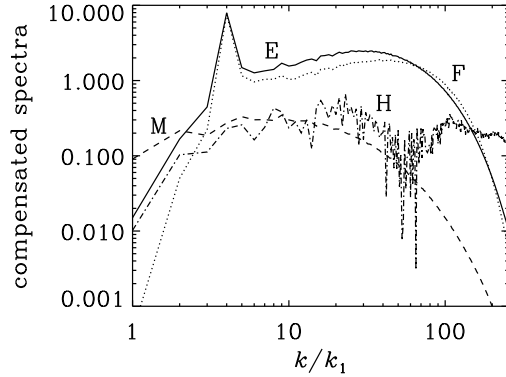


FIG. 6.— Compensated spectra of kinetic and magnetic energies and helicities in the kinematic regime for  $\text{Pr}_M = 1$ . The spectra are denoted by letters E, F, M, and H, as described in the text.

ent  $\text{Pr}_M$  to an arbitrarily chosen reference value of  $10^{-6}$  below the kinetic energy spectrum. For  $\text{Pr}_M = 1$  the magnetic energy seems to follow an approximate Kazantsev (1968) spectrum with a range proportional to  $k^{3/2}$  and is peaked at the resistive scale near  $k/k_1 = 50$ . For smaller values of  $\text{Pr}_M$  the peak of magnetic energy moves to smaller wavenumbers.

In order to judge the correspondence with various power-law scalings we label, in Fig. 6, various compensated spectra as follows:

$$\text{label E : } E(k)\epsilon_K^{-2/3}k^{5/3}, \quad (6)$$

$$\text{label F : } |F(k)|\epsilon_K^{-2/3}k^{5/3}/2k_f, \quad (7)$$

$$\text{label M : } M(k)k_f(k/k_*)^{-3/2}/M, \quad (8)$$

$$\text{label H : } |H(k)|k_f\epsilon_K^{-2/3}k^{5/3}E/2M, \quad (9)$$

where  $k_* = \int kM(k)dk/M$  is the wavenumber where the magnetic energy spectrum peaks and  $\epsilon_K$  is the kinetic energy dissipation per unit mass. The compensated kinetic energy spectrum shows a bottleneck that is clearly stronger than in the case without helicity (e.g., Kaneda et al. 2003, Haugen & Brandenburg 2006). The kinetic helicity spectrum shows a similar spectrum that also has a strong bottleneck, which is particularly evident when it is compensated by  $k^{5/3}$ . The existence of a  $k^{5/3}$  subrange for the modulus of the kinetic

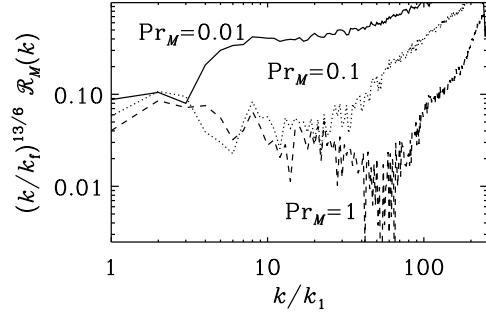


FIG. 7.— Relative spectral magnetic helicity,  $k|H(k)|/2M(k)$ , compensated by  $(k/k_f)^{13/6}$ , for  $\text{Pr}_M$  ranging from  $0.01$  to  $1$ .

helicity spectrum is well known from early closure calculations (André & Lesieur 1977), and has also been seen in direct numerical simulations (Borue & Orszag 1997, Brandenburg & Subramanian 2005a) and in shell model calculations (Ditlevsen & Giuliani 2001). Such a scaling implies that the relative spectral kinetic helicity,

$$\mathcal{R}_K(k) \equiv F(k)/2kE(k), \quad (10)$$

decreases toward small scales like  $k^{-1}$  and has a maximum at  $k = k_f$  with  $\mathcal{R}_K(k_f) = 0.96$ . At that scale, the relative magnetic helicity,

$$\mathcal{R}_M(k) \equiv kH(k)/2M(k), \quad (11)$$

is  $-0.15, -0.08,$  and  $+0.42$  for  $\text{Pr}_M = 1, 0.1,$  and  $0.01$ , respectively. The realizability condition implies that the moduli of  $\mathcal{R}_K(k)$  and  $\mathcal{R}_M(k)$  are less than unity (Moffatt 1969). The positive sign for  $\text{Pr}_M = 0.01$  agrees with the idea that the helical driving of the flow imprints a helical field of the same sense at the same scale. Owing to an inverse cascade of magnetic helicity (Pouquet et al. 1976),  $H(k)$  is of opposite sign at large scales. While this is very clearly established in the nonlinear regime (B01) or for small values of  $\text{Pr}_M$ , a larger range of scales attains negative values during the linear stage when  $\text{Pr}_M = 0.1$  and  $1$ .

For the magnetic helicity we also find an approximate  $|H(k)| \sim k^{-5/3}$  spectrum, which is different from the nonlinear case when the current helicity,  $C(k) = k^2H(k)$  shows a  $k^{-5/3}$  spectrum (Brandenburg & Subramanian 2005a). Assuming that  $M(k) \sim k^{3/2}$ , the relative spectral helicity would seem to decrease now more rapidly like  $k|H(k)|/2M(k) \sim k^{-13/6}$ . Figure 7 shows that the correspondingly compensated magnetic helicity to energy ratio changes now less strongly in the range  $4 \leq k/k_1 \leq 40$ .

### 3.4. Saturation regime

Eventually the initial exponential growth comes to a halt and is followed by a resistively long saturation phase during which a large-scale magnetic field develops at wavenumber  $k_1$ , regardless of the value of  $k_f$ . Owing to the use of periodic boundary conditions, this large-scale field tends to be force-free and fully helical, and its energy per unit volume is by a factor  $k_f/k_1 = 4$  larger than the value at  $k_f$ , which in turn is comparable to the kinetic energy per unit volume. For details see B01. Here we only consider the end of this slow saturation phase. Compensated kinetic and magnetic energy spectra are shown in Fig. 8 for magnetic Prandtl numbers ranging from  $1$  to down to  $10^{-3}$ .

In the final saturated state, and especially for  $\text{Pr}_M = 1$ , the  $M(k)$  and  $E(k)$  spectra are nearly on top of each other with  $M(k)$  being slightly larger than  $E(k)$  by 20%, which is qualitatively similar to the non-helical case (cf. Haugen et al. 2003). There are indications of a somewhat shallower spectrum due to a bottleneck effect both for kinetic and magnetic energies just before the two enter the viscous and resistive dissipation ranges. Also for  $\text{Pr}_M = 0.1$  there is a short range where  $M(k)$  exceeds  $E(k)$ , but then, not surprisingly,  $M(k)$  turns into the dissipation range before  $E(k)$  does. This is even more clearly the case for  $\text{Pr}_M = 0.01$ .

Low- $\text{Pr}_M$  turbulence has the interesting property that for given numerical resolution much larger fluid Reynolds numbers can be achieved than for  $\text{Pr}_M = 1$ . This is simply because almost all the energy is dissipated resistively, and the energy that continues along the kinetic energy cascade is comparatively weak, so not much viscosity is needed for dissipating the remaining kinetic energy. In fact, for  $\text{Pr}_M = 0.01$  we were able to go to  $\text{Re} = 2300$  with a resolution of only  $512^3$  mesh-points. For  $\text{Pr}_M = 0.1$  and 1 and the same resolution we could only go to  $\text{Re} = 1200$  and 450, respectively.

### 3.5. Diverting most of the energy into Joule heat

As has recently been stressed by Mininni (2007), an increasing fraction of energy is being dissipated via Joule dissipation, as  $\text{Pr}_M$  decreases. In Fig. 9, we plot the dependence of the kinetic and magnetic energy dissipation rates per unit mass,  $\epsilon_K = \langle 2\rho\mathbf{v}\mathbf{S}^2 \rangle / \rho_0$  and  $\epsilon_M = \langle \eta\mu_0\mathbf{J}^2 \rangle / \rho_0$ , relative to the total dissipation,  $\epsilon_T = \epsilon_K + \epsilon_M$ , versus  $\text{Pr}_M$ . The data are well described by a power-law fit of the form

$$\epsilon_K / \epsilon_T \approx 0.37 \text{Pr}_M^{1/2}. \quad (12)$$

Thus, for  $\text{Pr}_M = 1$  about the 37% of the energy is dissipated into viscous heat, while 63% is dissipated via Joule dissipation. This is similar to the case of non-helical hydromagnetic turbulence (Haugen et al. 2003), where these numbers are about 30% and 70%, respectively.

In turbulence the energy dissipation is generally proportional to  $U^3/L$ , where  $U$  is the typical velocity and  $L$  is a typical length scale. Conventionally one defines a dimensionless dissipation parameter as

$$C_\epsilon = \frac{\epsilon_T}{U^3/L}, \quad (13)$$

where  $U$  is the one-dimensional rms velocity, which is related to  $u_{\text{rms}}$  via  $U^2 = u_{\text{rms}}^2/3$ , and  $L$  is the integral scale and is related to  $k_f$  via  $\frac{3}{4}\pi/k_f$ . In non-helical turbulence this value is typically around 0.5 (see also Pearson et al. 2004), but this value has never been determined for hydromagnetic turbulence with helicity. An exception is the work of Blackman & Field (2008), who considered a range of power-law scalings for kinetic and magnetic energy spectra to calculate analytically the dissipation rates.

It turns out that for our runs,  $C_\epsilon \approx 1.5$ , i.e.  $\approx 3$  times larger than the usual value; see Fig. 10. Let us now discuss possible reasons for this difference. In the definition of the quantity  $C_\epsilon$  one assumes that the energy flux scales with  $U^3/L$ . However,  $U$  is based on the typical rms velocity. In the presence of a strong dynamo-generated magnetic field it may be sensible to base it on a combination of typical velocity and magnetic field strength. In our case we have  $\langle \mathbf{B}^2 / \mu_0 \rangle / \langle \rho \mathbf{U}^2 \rangle \approx 2$ , so  $U$  would need to be scaled up by a factor  $\sqrt{3}$ , which reduces  $C_\epsilon$  by a factor  $3^{3/2} \approx 5$  to about 0.3. This value is nearly independent

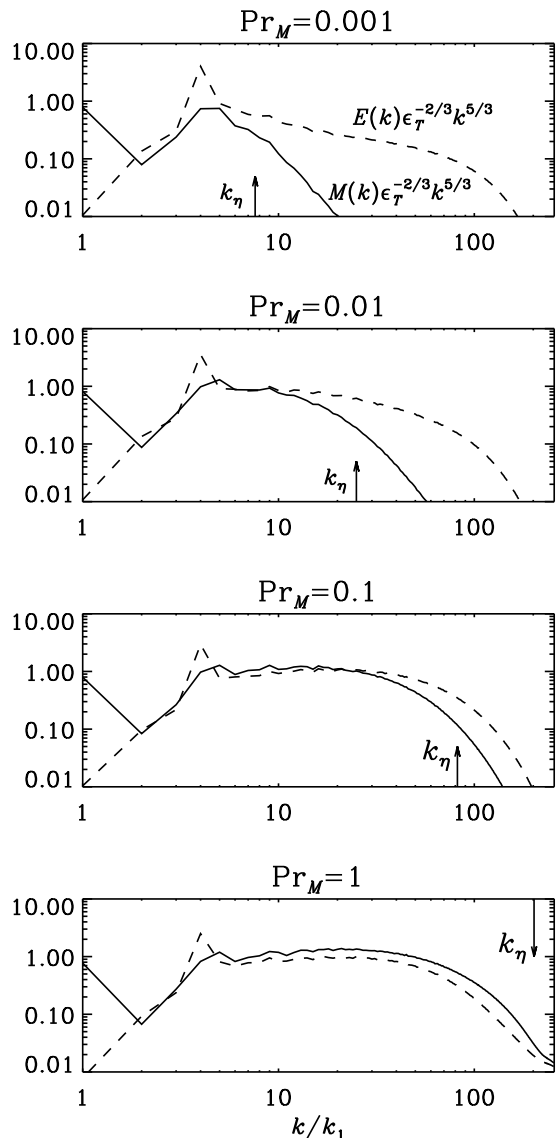


FIG. 8.— Kinetic and magnetic energy spectra in the saturated regime for  $\text{Pr}_M = 10^{-3}$  with  $\text{Re} = 4400$ ,  $\text{Pr}_M = 10^{-2}$  with  $\text{Re} = 2300$ ,  $\text{Pr}_M = 0.1$  with  $\text{Re} = 1200$ , and  $\text{Pr}_M = 1$  with  $\text{Re} = 450$ . All spectra are compensated by  $\epsilon_T^{-2/3} k^{5/3}$ . The ohmic dissipation wavenumber,  $k_\eta = (\epsilon_M/\eta^3)^{1/4}$ , is indicated by an arrow. The viscous dissipation wavenumbers are 430, 350, 290, and 180 for  $\text{Pr}_M = 10^{-3}$ ,  $10^{-2}$ , 0.1, and 1, respectively.

of the value of  $\text{Pr}_M$ , which was also found by Blackman & Field (2008) under plausible assumptions.

### 3.6. Helicity spectra

As mentioned before, in the nonlinear regime both kinetic and current helicities,  $F(k)$  and  $C(k) = k^2 H(k)$ , respectively, are expected to display a forward cascade with a  $k^{-5/3}$  spectrum. If this is true, we would expect that within some wavenumber interval  $|\mathcal{R}_K(k)|$  and  $|\mathcal{R}_M(k)|$  decrease with increasing  $k$  like  $k^{-1}$ . In Fig. 11 we show the correspondingly compensated relative kinetic and magnetic helicity spectra. It turns out that they are surprisingly similar regardless of the value of  $\text{Pr}_M$ . For  $\text{Pr}_M = 1$  and 0.1 the compensated profiles of  $\mathcal{R}_M(k)$  and  $\mathcal{R}_K(k)$  are reasonably flat in the range  $6 \leq k/k_1 \leq 14$ . However, for  $\text{Pr}_M = 10^{-2}$  and  $10^{-3}$  the compensated profiles show an increase proportional to  $k^{1/2}$ . The fact that the anticipated  $k^{-1}$  scaling occurs only for magnetic

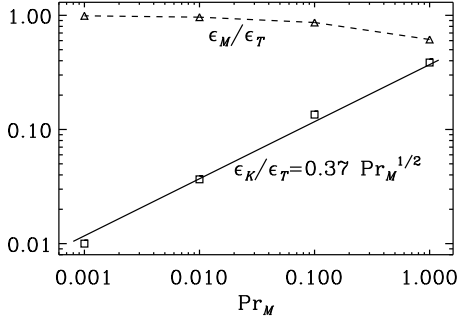


FIG. 9.— Dependence of the fractional kinetic and magnetic energy dissipation rates. Note that the fractional kinetic energy dissipation decreases with decreasing  $Pr_M$  to the  $1/2$  power.

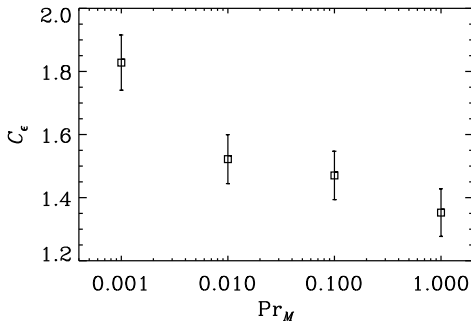


FIG. 10.— Dimensionless total energy dissipation rate,  $C_e$ , as a function of  $Pr_M$ . Error bars have been estimated based on averages taken over each third of the full time series.

Prandtl numbers down to 0.1 and only over an extremely short range may indicate that our Reynolds numbers are still too small to yield conclusive results. Especially at smaller scales, and certainly in the runs with the smallest  $Pr_M$ , the compensated relative kinetic and magnetic helicity spectra are compatible with a  $k^{1/2}$  slope. This would imply a  $k^{-7/6}$  spectrum for the kinetic and current helicities, which is shallower than that anticipated for a forward cascade, but still steeper than that in the case of equipartition. We emphasize again that this applies to the resistively controlled regime.

In Fig. 11 we see that at  $k = k_f$  both  $\mathcal{R}_K$  and  $\mathcal{R}_M$  are close to unity. This indicates that velocity and magnetic fields are nearly fully helical. However, for  $k > k_f$  the velocity and magnetic fields become less helical, because the compensated relative helicities in Fig. 11 increase with  $k$  not faster than to the  $1/2$  power. On the other hand, for  $k = k_1$  the magnetic field is again fully helical, i.e.  $(k_1/k_f)|\mathcal{R}_M(k_1)|$  is equal to  $k_1/k_f = 1/4$ , but its helicity has the opposite sign.

In Table 1 we compare the values of  $\mathcal{R}_M(k)$  during the linear and nonlinear stages at the wavenumbers  $k_1$  and  $k_f$  for the three or four values of  $Pr_M$ . Note that during the nonlinear stage  $\mathcal{R}_M(k_1)$  and  $\mathcal{R}_M(k_f)$  are of opposite sign. The former is close to  $-1$  while the latter increases from 0.52 to 0.72 as  $Pr_M$  decreases. As already indicated in §3.3, during the linear stage, the two are of opposite sign only for  $Pr_M = 0.01$ , while for larger values of  $Pr_M$  a larger range of scales appears to be affected by the inverse transfer of magnetic helicity causing  $\mathcal{R}_M(k_f)$  to be negative. It would be tempting to try and

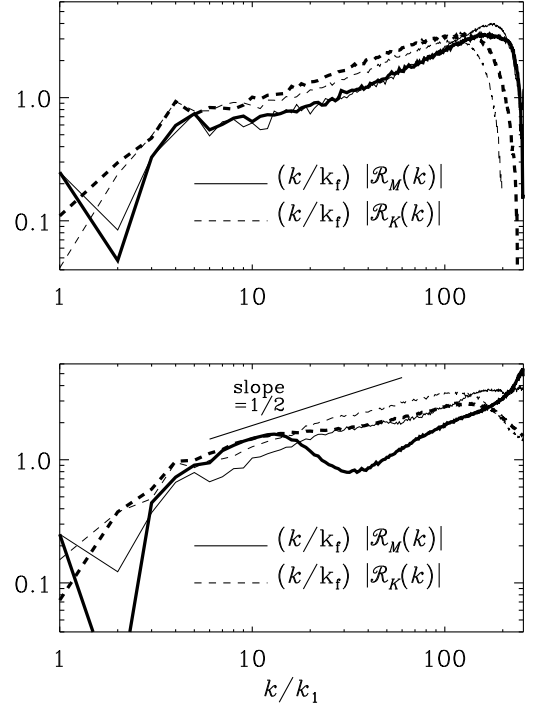


FIG. 11.— Spectral current and kinetic helicity ratios for the same four runs shown in Fig. 8. The upper panel is for  $Pr_M = 1$  (thin line) and 0.1 (thick line), while the lower panel is for  $10^{-2}$  (thin line) and  $10^{-3}$  (thick line). Note that for  $Pr_M = 1$  and 0.1 the profiles of  $(k/k_f)|\mathcal{R}_M(k)|$  and  $(k/k_f)|\mathcal{R}_K(k)|$  are reasonably flat in the range  $6 \leq k/k_1 \leq 14$ . The  $1/2$  slope is shown for comparison.

model this behavior using, for example, the four-scale helical dynamo model of Blackman (2003).

TABLE 1  
COMPARISON OF  $\mathcal{R}_M(k_1)$  AND  $\mathcal{R}_M(k_f)$  DURING THE LINEAR AND NONLINEAR STAGES FOR DIFFERENT VALUES OF  $Pr_M$ .

$Pr_M$	linear		nonlinear	
	$k_1$	$k_f$	$k_1$	$k_f$
$10^{-3}$			-0.993	+0.72
$10^{-2}$	-0.88	+0.42	-0.994	+0.66
$10^{-1}$	-0.59	-0.08	-0.993	+0.59
1	-0.41	-0.15	-0.993	+0.52

### 3.7. Effects on the velocity pattern

In Fig. 12 we compare visualizations of  $B_z$  and  $U_z$  for all four values of  $Pr_M$ . The velocity and magnetic field patterns are surprisingly similar for all four values of  $Pr_M$ . Only for  $Pr_M = 10^{-2}$  and  $10^{-3}$  the magnetic field appears noticeably smoother than in the other two cases. The velocity field shows a marked anisotropy with small-scale elongated patterns aligned with the local direction of the mean magnetic field, which is here of the form  $\bar{\mathbf{B}} \sim (0, \sin k_1 x, -\cos k_1 x)$ . The anisotropy in the velocity can still be seen for small values of  $Pr_M$ , but the small-scale patterns are slightly smoother.

## 4. CONCLUSIONS

In many astrophysical bodies the magnetic Prandtl number is small, while in most simulations its value is chosen to be

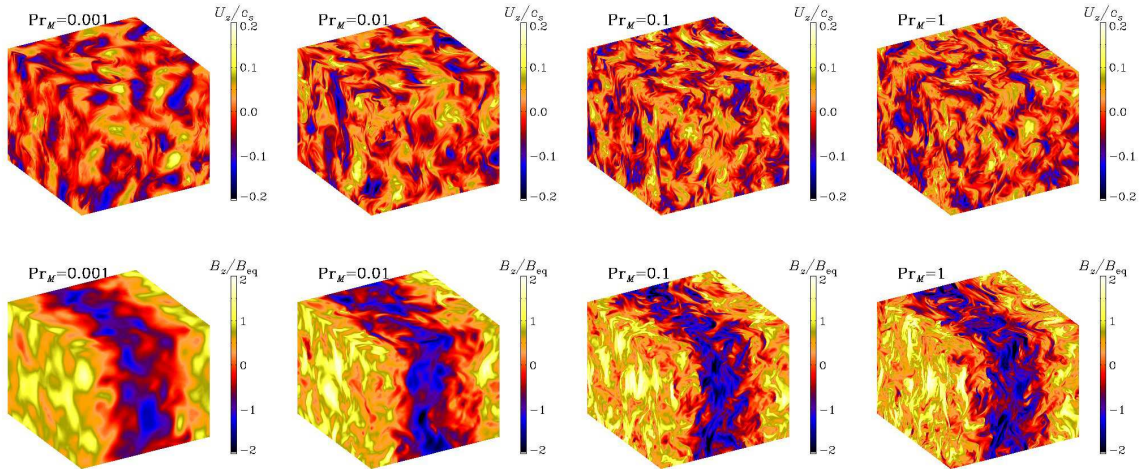


FIG. 12.— Visualizations of  $B_z$  and  $U_z$  for  $\text{Pr}_M = 10^{-3}$  at  $\text{Re} = 4400$  (left),  $\text{Pr}_M = 10^{-2}$  at  $\text{Re} = 2300$ ,  $\text{Pr}_M = 0.1$  at  $\text{Re} = 1200$ , and  $\text{Pr}_M = 1$  at  $\text{Re} = 450$  (right). The orientation of the axes is the same as in Fig. 1.

close to unity. As we have shown here, this mismatch is of relatively minor consequence for large-scale dynamos that are driven by helical forcing.

In the nonlinear stage, the velocity and magnetic field patterns are remarkably independent of the value of  $\text{Pr}_M$ . The only thing that changes is the length of the inertial range. A small magnetic Prandtl number simply means that the magnetic energy spectrum turns into the dissipation range more quickly than the kinetic energy spectrum. It also means that essentially all the energy is dissipated via Joule heat. This was recently also demonstrated by Mininni (2007). One reason is that the case of fully helical turbulence studied in the present paper is a particularly simple one, because it leads to uniform mean-field dynamo action with large-scale pattern formation covering the entire domain. In this paper we have seen that, at least for values of  $\text{Re}$  up to 4400, the dynamics of this large-scale pattern, i.e., of the large-scale magnetic field, is quite independent of how long the inertial range of the turbulence is. In the absence of helicity, there is only small-scale dynamo action, which is driven by the dynamics at the smallest possible scale, i.e. the resistive scale. In that case it does matter what the dynamics of the turbulence is at that scale. However, in that case it has not yet been possible to find dynamo action for values of  $\text{Pr}_M$  down to the values considered here. Nevertheless, it is possible that even in that case there is an asymptotic regime for large enough values of  $\text{Re}_M$  where the dynamics of the magnetic field is independent of the value of  $\text{Pr}_M$ , even though this regime is not yet accessible with present day computers.

To estimate the value of the magnetic Prandtl number in dense astrophysical bodies, one has to use the *Spitzer* formulae for  $\eta$  and  $\nu$ . The resulting magnetic Prandtl number is (e.g., Brandenburg & Subramanian 2005b)

$$\text{Pr}_M = 1.1 \times 10^{-4} \left( \frac{T}{10^6 \text{ K}} \right)^4 \left( \frac{\rho}{0.1 \text{ g cm}^{-3}} \right)^{-1} \left( \frac{\ln \Lambda}{20} \right)^{-2}, \quad (14)$$

so at the bottom of the solar convection zone the magnetic

Prandtl number is clearly rather small ( $\sim 10^{-4}$ ). Nevertheless, simulations of solar and stellar dynamos available so far  $\text{Pr}_M$  are set to values of the order or unity. Although we have shown here that the resulting large-scale fields are similar to the more realistic case of small values of  $\text{Pr}_M$ , an important difference is that the small-scale dynamo may be more pronounced when  $\text{Pr}_M$  is of order unity. In practice this means that a positive detection of dynamo action in a simulation might not necessarily be relevant for understanding the Sun, unless suitable conditions for the excitation of large-scale dynamo action are also met. On the other hand, once the large-scale dynamo is really excited, and if it is fully saturated, it is then quite feasible to lower the value of  $\text{Pr}_M$  significantly—without losing the large-scale dynamo. In fact, lowering  $\text{Pr}_M$  in a saturated large-scale dynamo means that most of the energy will be dissipated via Joule heating, and that the kinetic energy cascade only carries a small fraction of the total energy. This allows us to increase the value of  $\text{Re}$ , and hence to decrease the viscosity and thereby the value of  $\text{Pr}_M$  even further. Simulations of large-scale dynamo action in turbulent convection (Käpylä et al. 2008) provide one example where it is indeed feasible to lower  $\text{Pr}_M$ , although in that case the system is not uniform and so energy dissipation via Joule heating is only possible in those locations where the dynamo is strong enough (P. J. Käpylä 2008, private communication).

I thank Eric G. Blackman and Pablo Mininni for useful comments on the paper, and an anonymous referee for spotting a number of errors in the original version. It is a pleasure to acknowledge the organizers of the KITP program on dynamo theory and the staff of the KITP for providing a stimulating atmosphere. This research was supported in part by the National Science Foundation under grant PHY05-51164 and the Swedish Research Council under grant 621-2007-4064. The computations have been carried out at the National Supercomputer Centre in Linköping and at the Center for Parallel Computers at the Royal Institute of Technology in Sweden.

#### REFERENCES

André, J.-C. & Lesieur, M. 1977, *J. Fluid Mech.*, 81, 187  
 Borue, V., & Orszag, S. A. 1997, *Phys. Rev. E*, 55, 7005

Blackman, E. G. 2003, *MNRAS*, 344, 707  
 Blackman, E. G., & Field, G. B. 2008, *MNRAS*, 386, 1481

- Boldyrev, S., & Cattaneo, F. 2004, *Phys. Rev. Lett.*, 92, 144501
- Brandenburg, A. 2001, *ApJ*, 550, 824
- Brandenburg, A., Rädler, K.-H., Rheinhardt, M., & Subramanian, K. 2008, *ApJ*, 687, L49
- Brandenburg, A., & Subramanian, K. 2005a, *A&A*, 439, 835
- Brandenburg, A., & Subramanian, K. 2005b, *Phys. Rep.*, 417, 1
- Ditlevsen, P. D., & Giuliani, P. 2001, *Phys. Rev. E*, 63, 036304
- Dobler, W., Haugen, N. E. L., Yousef, T. A., & Brandenburg, A. 2003, *Phys. Rev. E*, 68, 026304
- Haugen, N. E. L., Brandenburg, A., & Dobler, W. 2003, *ApJ*, 597, L141
- Haugen, N. E. L., Brandenburg, A., & Dobler, W. 2004, *Phys. Rev. E*, 70, 016308
- Haugen, N. E. L., & Brandenburg, A. 2006, *Phys. Fluids*, 18, 075106
- Hubbard, A., & Brandenburg, A. 2008, *ApJ*, submitted, arXiv:0811.2561
- Iskakov, A. B., Schekochihin, A. A., Cowley, S. C., McWilliams, J. C., Proctor, M. R. E. 2007, *Phys. Rev. Lett.*, 98, 208501
- Kaneda, Y., Ishihara, T., Yokokawa, M., Itakura, K., & Uno, A. 2003, *Phys. Fluids*, 15, L21
- Käpylä, P. J., Korpi, M. J., & Brandenburg, A. 2008, *A&A*, 491, 353
- Kazantsev, A. P. 1968, *Sov. Phys. JETP*, 26, 1031
- Krause, F., & Rädler, K.-H. 1980, *Mean-field magnetohydrodynamics and dynamo theory* (Pergamon Press, Oxford)
- Mininni, P. D. 2007, *Phys. Rev. E*, 76, 026316
- Moffatt, H. K. 1969, *J. Fluid Mech.*, 35, 117
- Moffatt, H. K. 1978, *Magnetic field generation in electrically conducting fluids* (Cambridge University Press, Cambridge)
- Pearson, B. R., Yousef, T. A., Haugen, N. E. L., Brandenburg, A., & Krogstad, P. Å. 2004, *Phys. Rev. E*, 70, 056301
- Ponty, Y., Mininni, P. D., Montgomery, D. C., Pinton, J.-F., Politano, H., Pouquet, A. 2005, *Phys. Rev. Lett.*, 94, 164502
- Ponty, Y., Politano, H., & Pinton, J.-F. 2004, *Phys. Rev. Lett.*, 92, 144503
- Pouquet, A., Frisch, U., & Léorat, J. 1976, *J. Fluid Mech.*, 77, 321
- Rogachevskii, I., & Kleorin, N. 1997, *Phys. Rev. E*, 56, 417
- Schekochihin, A. A., Cowley, S. C., Taylor, S. F., Maron, J. L., McWilliams, J. C. 2004, *ApJ*, 612, 276
- Schekochihin, A. A., Haugen, N. E. L., Brandenburg, A., Cowley, S. C., Maron, J. L., & McWilliams, J. C. 2005, *ApJ*, 625, L115
- Sur, S., Brandenburg, A., & Subramanian, K. 2008, *MNRAS*, 385, L15